

Modeling and Analysis of MMC-Based HVDC Effect on Subsynchronous Torsional Stability

S. Al-Areqi, P. Correa, M. Dommaschk, J. Rittiger, S. Teeuwsen, and A. Chaudhry

Abstract—With the rapidly increasing penetration of power-electronic based renewable energy generation units, new opportunities and challenges have been raised. Among others, the challenges result from their interactions with nearby existing turbine generators in the subsynchronous frequency range. A design strategy which considers the impact of such interactions on stability of the subsynchronous oscillations is of special importance. For this purpose, a simple approach of modeling and analyzing MMC-based HVDC systems with the aforementioned challenges is proposed in this paper. The proposed approach is characterized by considering a so-called emulation-based design strategy. A condition of stability is derived from the Nyquist criterion for stable open-loop transfer functions. Its effectiveness is evaluated for a detailed representation of the system under study in the PSCAD environment.

Keywords—Subsynchronous resonance (SSR), modular multilevel converter (MMC), high-voltage direct current (HVDC), subsynchronous torsional interaction (SSTI), IEEE first benchmark model (FBM).

I. INTRODUCTION

ANALYSIS of subsynchronous resonance (SSR) in power systems has been received considerable attention both in academia as well as in industry. This is witnessed by several publications in literature, see e.g. the monographs [1], [2], [3] and the survey paper [4]. Among others, the torsional interaction effect between the active control units of an HVDC and long shafts of nearby turbine generators might cause such SSR issues. Depending on the control structure and the control setting, the natural torsional frequencies of the combined system might be excited in an unstable manner. Due to the current trend of power-electronic based renewable energy generation units, the impact of such devices on stability of the subsynchronous oscillations becomes a very important research topic.

Since the subsynchronous torsional interaction (SSTI) is a steady-state phenomenon, many approaches based on small-signal analysis have been proposed in literature [5], [6], [7], [8], [9], [10], [11], [12], [13], [14]. Most of the aforesaid approaches are based on the partition of the system under study into a mechanical part and an electrical part. The impedance of each is first determined and the impedance ratio is then used to judge the stability of each torsional mode. The interaction of the converter station with the ac system is thus characterized by its impedance, as seen from the ac system. The shape of this impedance depends on the chosen control structure as well as on the chosen control

parameters. The impedance-based stability analysis has been applied to different power electronic devices, including wind turbines [13], PV inverters [9], HVDC converters [10], [5], and STATCOM [8]. Due to the fact that almost all power electronic circuits are nonlinear, the impedance-based linear representation is only valid for small-signal analysis.

Modeling and control of HVDC systems are usually conducted in the rotating dq -frame. This allows the further use of the conventional small-signal analysis tools and techniques. Even if the resulting converter impedance matrix is diagonal or diagonalizable, the effective impedance of the generator is usually a full square matrix. Integrating both impedances leads to a coupling between the d -component and the q -component dynamics, making the stability analysis a very difficult task. The analysis is usually performed numerically and hence no way to see the effects of individual components and design parameters on stability.

In order to cope with the underlying difficulty, a simple analytical approach of modeling and analyzing the stability based on the Nyquist theory for single-input single-output (SISO) systems is proposed in this paper. A mathematical model of the MMC-based HVDC system, as shown in Figure 1, is first derived. Further details on the system architecture are given in the following section.

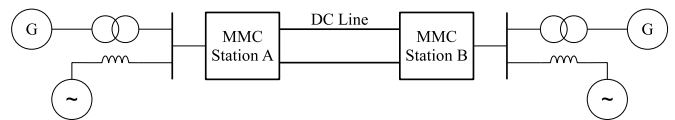


Figure 1. Schematic diagram of an MMC-based HVDC system

The resulting nonlinear model is then linearized about an initial operating condition for further small-signal analysis. Based on the linearized model, an emulation-based design method [15] is considered. Emulation-based design is a two-step design procedure with which a controller of the HVDC is first determined using classical control theory („design step“) and then the stability of the closed-loop system taking the mechanical dynamics of the turbine generator explicitly into account is studied („implementation step“). A condition of stability for the d -component as well as for the q -component is followed from the Nyquist criterion for stable open-loop transfer functions. The proposed stability condition allows invaluable insight into the effect of the controller as well as of the dq -coupling terms on the stability. The

The authors are with the Siemens AG, Energy Management Division, Transmission Solutions, Freylebenstraße 1, 91058 Erlangen, Germany (E-mail of corresponding author: sanad.al-areqi@siemens.com).

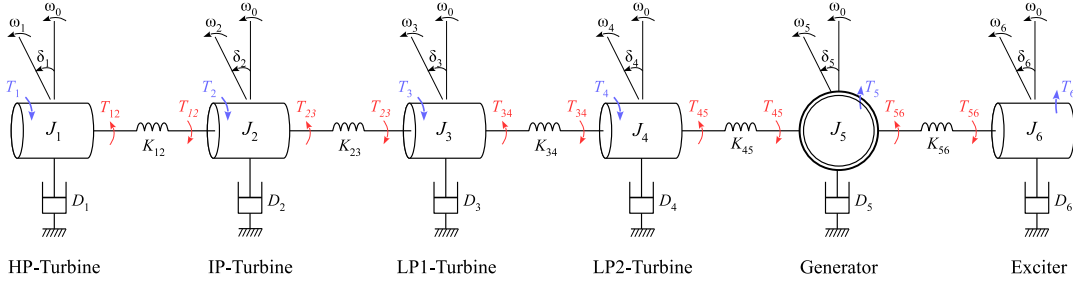


Figure 2. IEEE first benchmark model of the rotor system

effectiveness of the proposed theory is finally evaluated for a case study.

Throughout the paper the following notation is used: Scalars are denoted by lower- and upper-case non-bold letters (a, b, \dots, A, B, \dots), vectors by lower-case bold letters ($\mathbf{a}, \mathbf{b}, \dots$), matrices by upper-case bold letters ($\mathbf{A}, \mathbf{B}, \dots$), and sets by upper-case double-struck letters ($\mathbb{A}, \mathbb{B}, \dots$). Finally, \mathbf{A}^{-1} denotes the inverse of matrix \mathbf{A} and \mathbb{R}_0^+ the set of non-negative real scalars.

II. MODELING

A. System Architecture

Consider the MMC-based HVDC system shown in Figure 1. It consists of two stations, namely Station A on the left-hand side and Station B on the right-hand side. Each station is connected from its ac side through a common busbar with a simplified ac network. The ac network is represented with an infinite source in series with an output impedance and a generator in series with a power transformer. The strength of the ac network, as seen from the converter station, can be changed by varying the output impedance of the infinite source. The rotor of the generator is represented with a multi-mass model, details on the multi-mass model are given in the following section. Finally, a dc transmission line (cable, overhead, or combination of both) is connecting each dc pole with its counterpart.

The following derivation of the ac system's mathematical model is splitted into two parts, namely mechanical part and electrical part. Furthermore, the branch that includes the infinite source and its corresponding output impedance is neglected in the following for simplicity of presentation without loss of generality. By doing so, the positive damping contribution of the output impedance on the torsional oscillations is neglected, focusing only on the effect of the converter station. From this perspective, the proposed analysis in this paper considers worst-case conditions concerning the subsynchronous torsional stability.

B. Mechanical Part

The focus in this section is on the modeling of the rotor system of the turbine generator under study. The IEEE first benchmark model [16] for the study of subsynchronous

resonance is considered, as shown in Figure 2. The equations of motion of the utilized multi-mass model are given by

$$\begin{aligned}
 J_1 \frac{d^2 \delta_1}{dt^2} &= T_1 - K_{12}(\delta_1 - \delta_2) - D_1 \cdot \Delta \omega_1 \\
 J_2 \frac{d^2 \delta_2}{dt^2} &= T_2 + K_{12}(\delta_1 - \delta_2) - K_{23}(\delta_2 - \delta_3) - D_2 \cdot \Delta \omega_2 \\
 J_3 \frac{d^2 \delta_3}{dt^2} &= T_3 + K_{23}(\delta_2 - \delta_3) - K_{34}(\delta_3 - \delta_4) - D_3 \cdot \Delta \omega_3 \\
 J_4 \frac{d^2 \delta_4}{dt^2} &= T_4 + K_{34}(\delta_3 - \delta_4) - K_{45}(\delta_4 - \delta_5) - D_4 \cdot \Delta \omega_4 \\
 J_5 \frac{d^2 \delta_5}{dt^2} &= K_{45}(\delta_4 - \delta_5) - T_5 - K_{56}(\delta_5 - \delta_6) - D_5 \cdot \Delta \omega_5 \\
 J_6 \frac{d^2 \delta_6}{dt^2} &= K_{56}(\delta_5 - \delta_6) - T_6 - D_6 \cdot \Delta \omega_6
 \end{aligned}$$

with the parameters described in Table I $\forall i, j \in \{1, \dots, 6\}$.

TABLE I
PARAMETER DESCRIPTION FOR THE MULTI-MASS MODEL

Parameter	Description	Unit
J_i	Moment of inertia	kg.m ²
T_i	Torque applied to mass i	N.m
D_i	Damping coefficient	N.m.s/rad
K_{ij}	Shaft stiffness	N.m/rad
δ_i	Angular position of mass $i = \omega_i t - \omega_0 t$	rad
ω_i	Speed of mass i	rad/s
ω_0	Rated speed of mass i	rad/s
$\Delta \omega_i$	Speed deviation of mass $i = \omega_i - \omega_0$	rad/s

The corresponding mechanical transfer function to be used later on in the stability analysis is thus given by

$$G_m(s) = \frac{\delta_5(s)}{T_5(s)} = \frac{\delta(s)}{T_e(s)} \quad (1)$$

with the rotor angle δ and the generator air-gap torque T_e .

C. Electrical Part

For the electrical part, a simplified transient model of the generator (classical model) is considered [1, Sec. 5.3.1]. The generator is modeled as a fixed voltage source \mathbf{u}_{gen} behind an output impedance \mathbf{Z}_{gen} . The magnitude \hat{u} and the frequency ω_0 of the voltage source are assumed to be constant while using its angle with respect to a synchronously rotating reference frame as a measure of the rotor angle δ . The same simplification applies to the converter station, which can be modeled as a

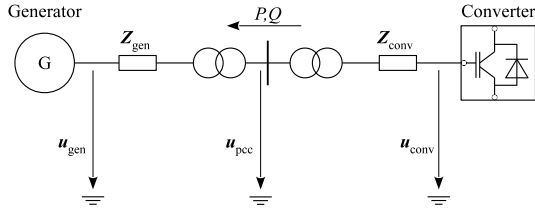


Figure 3. Single-line diagram of the electrical model

controlled voltage source \mathbf{u}_{conv} behind an output impedance \mathbf{Z}_{conv} . The converter is connected to the common busbar via a power transformer as well. A single line diagram of the resulting electrical model is illustrated in Figure 3. Note that the active control units of the converter are not yet considered.

Applying the Kirchhoff's voltage law to the electrical model in Figure 3 leads in the rotating dq -frame to the electrical transfer function matrix

$$\mathbf{G}_e(s) = \frac{\mathbf{i}_{dq}(s)}{\mathbf{u}_{dq}(s)} \quad (2)$$

where $\mathbf{i}_{dq}(s)$ is the current flowing from the converter towards the generator and $\mathbf{u}_{dq}(s) = \mathbf{u}_{\text{conv}}(s) - \mathbf{u}_{\text{gen}}(s)$ is the voltage difference between the converter and the generator. As a reference for the dq -transformation, the common busbar voltage \mathbf{u}_{pcc} has been chosen. Integrating the mechanical model (1) with the electrical model (2) yields finally the overall model of the ac system as shown in Figure 4.

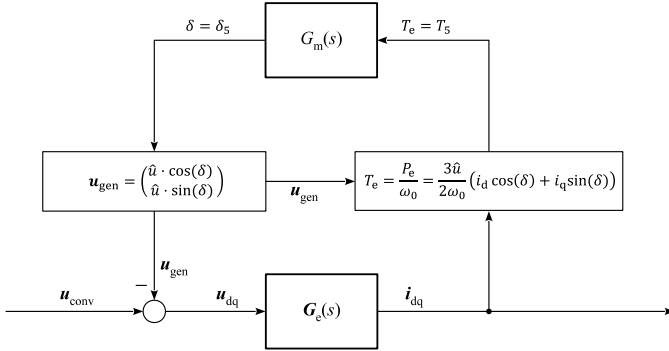


Figure 4. Block diagram of the ac system's overall model

Although the resulting mechanical and electrical models are linear time-invariant, the resulting overall model is due to the generator's torque/voltage equation unfortunately nonlinear. For the purpose of analyzing the stability in the frequency domain, the overall model is linearized about an initial operating condition in the following section.

III. STABILITY ANALYSIS

Consider the well-known standard control structure shown in Figure 5 for modular multilevel converters [17], [18], with the decoupling matrix denoted by $\mathbf{L}(s)$ and the diagonal control matrix denoted by $\mathbf{K}_{\text{diag}}(s)$. The control parameters

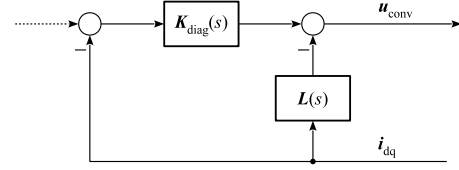


Figure 5. Block diagram of the standard control structure

are determined by only taking the electrical transfer function matrix defined in (2) into account, i.e. emulation-based design.

The inner loop composing of the electrical transfer function matrix $\mathbf{G}_e(s)$ and the decoupling matrix $\mathbf{L}(s)$ yields a diagonal matrix

$$\mathbf{G}_{\text{diag}}(s) = \mathbf{G}_e(s) \cdot (\mathbf{I} + \mathbf{L}(s)\mathbf{G}_e(s))^{-1}. \quad (3)$$

The outer loop composing of the diagonal matrix $\mathbf{G}_{\text{diag}}(s)$ and the diagonal control matrix $\mathbf{K}_{\text{diag}}(s)$ yields further an electrical admittance matrix

$$\mathbf{H}_{\text{diag}}^{-1}(s) = \mathbf{G}_{\text{diag}}(s) \cdot (\mathbf{I} + \mathbf{K}_{\text{diag}}(s)\mathbf{G}_{\text{diag}}(s))^{-1}. \quad (4)$$

Linearizing the generator voltage equation defined in Figure 4 about an initial operating condition $\delta = \delta_0$ yields

$$\Delta \mathbf{u}_{\text{gen}} = \begin{pmatrix} -\hat{u} \sin(\delta_0) \cdot \Delta \delta \\ \hat{u} \cos(\delta_0) \cdot \Delta \delta \end{pmatrix}. \quad (5)$$

Linearizing further the electrical torque equation defined also in Figure 4 about an initial operating condition $\delta = \delta_0$, $i_d = i_{d0}$, and $i_q = i_{q0}$ yields

$$\Delta T_e = k_\delta \cdot \Delta \delta + k_d \cdot \Delta i_d + k_q \cdot \Delta i_q \quad (6)$$

where

$$k_\delta = \frac{\partial T_e}{\partial \delta} = \frac{3\hat{u}}{2\omega_0} \cdot (-\sin(\delta_0)i_{d0} + \cos(\delta_0)i_{q0})$$

$$k_d = \frac{\partial T_e}{\partial i_d} = \frac{3\hat{u}}{2\omega_0} \cdot \cos(\delta_0)$$

$$k_q = \frac{\partial T_e}{\partial i_q} = \frac{3\hat{u}}{2\omega_0} \cdot \sin(\delta_0).$$

The concatenation of the linearized voltage (5), the mechanical transfer function (1), and the linearized torque (6) yields a full impedance matrix

$$\mathbf{Z}_{\text{full}}(s) = \frac{\mathbf{u}_{\text{gen}}}{\mathbf{i}_{dq}} = \begin{pmatrix} Z_{11} & -Z_{12} \\ Z_{21} & Z_{22} \end{pmatrix}. \quad (7)$$

The resulting linearized closed-loop model is depicted in Figure 6 with the harmonic impedance $\mathbf{H}_{\text{diag}} = \text{diag}(H_d, H_q)$ and the effective generator impedance

$$Z_d = Z_{11} + Z_{12} \cdot (H_q + Z_{22})^{-1} \cdot Z_{21}$$

$$Z_q = Z_{22} + Z_{21} \cdot (H_d + Z_{11})^{-1} \cdot Z_{12}. \quad (8)$$

Assume that the full impedance matrix in (7) is internally stable, i.e. all transfer functions obtained from all input-output pairs have their poles in the left-half plane (input-output stable). Assume further that the admittance matrix (4) and the effective generator impedance (8) are also internally stable,

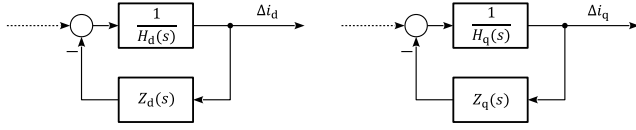


Figure 6. Block diagram of the linearized closed-loop model

as is usually the case. What left is just to prove the internal stability of the closed-loop model shown in Figure 6.

Theorem 1. *For the internally stable admittance matrix (4) and the effective generator impedance (8), the closed-loop model shown in Figure 6 is internally stable if $\forall \omega$ it holds*

$$\begin{aligned} \operatorname{Re}\{H_d(j\omega)\} &\geq 0 \quad \text{and} \quad \operatorname{Re}\{H_d(j\omega)\} + \operatorname{Re}\{Z_d(j\omega)\} > 0 \\ \operatorname{Re}\{H_q(j\omega)\} &\geq 0 \quad \text{and} \quad \operatorname{Re}\{H_q(j\omega)\} + \operatorname{Re}\{Z_q(j\omega)\} > 0 \end{aligned} \quad (9)$$

with $\operatorname{Re}\{\cdot\}$ denoting the real part of a complex number.

Proof. Due to their similarity, the proof is done in the following for the d -component only. The corresponding open-loop transfer function is given by

$$L_d(s) = \frac{1}{H_d(s)} \cdot Z_d(s) \quad (10)$$

The open-loop transfer function (10) is stable. According to the Nyquist criterion for stable open-loop transfer functions [19, Chapter 9], the closed-loop model is stable if and only if its Nyquist plot $1 + L_d(j\omega)$, $\forall \omega$, neither intersects the critical point $(0, j0)$ nor encircles it. This is equivalent for all ω to

$$1 + L_d(j\omega) \neq -\sigma \quad \forall \sigma \geq 0 \quad (11)$$

with the symbol σ denoting any non-negative real scalar $\sigma \in \mathbb{R}_0^+$. Substituting (10) with $s = j\omega$ into (11) leads $\forall \omega$ to

$$H_d(j\omega) + Z_d(j\omega) \neq -\sigma \cdot H_d(j\omega) \quad (12)$$

or equivalently,

$$\operatorname{Re}\{H_d(j\omega)\} + \operatorname{Re}\{Z_d(j\omega)\} \neq -\sigma \cdot \operatorname{Re}\{H_d(j\omega)\}. \quad (13)$$

The feasibility of (9) implies the feasibility of (13), completing thus the proof. \square

Remark 1. *For the special case of a strictly passive effective impedance $Z_d(s)$, i.e.*

$$\operatorname{Re}\{Z_d(j\omega)\} > 0 \quad \Leftrightarrow \quad |\angle Z_d(j\omega)| < 90^\circ \quad \forall \omega$$

the passivity [20], [21], [22] of the harmonic impedance $H_d(s)$, i.e.

$$\operatorname{Re}\{H_d(j\omega)\} \geq 0 \quad \Leftrightarrow \quad |\angle H_d(j\omega)| \leq 90^\circ \quad \forall \omega$$

guarantees, according to (9), the stability of the d -component closed-loop model shown in Figure 6. The same statement can be made for the q -component closed-loop model as well.

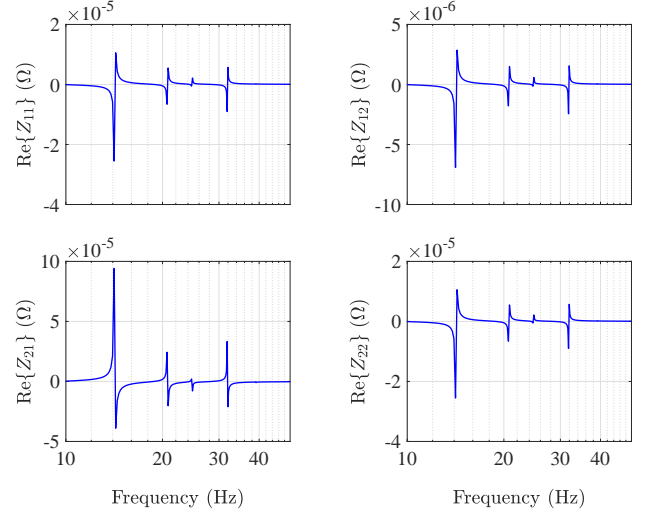


Figure 7. Real part of the resulting full impedance matrix \mathbf{Z}_{full}

IV. SIMULATION

A detailed representation of the MMC-based HVDC system, as shown in Figure 1, is implemented in the PSCAD environment. The mechanical torques between the masses of the multi-mass model, as shown in Figure 2, are monitored to demonstrate the effect of the converter's harmonic impedance on the subsynchronous torsional stability. The torsional frequencies of the multi-mass model are summarized in Table II.

TABLE II
TORSIONAL FREQUENCIES OF THE MULTI-MASS MODEL

Mode	Torsional Frequency in Hz
1	14.19
2	20.73
3	24.76
4	31.86
5	39.10

The operating condition of the generator is chosen as

$$\begin{aligned} \hat{u} &= 1.06 \text{ p.u.} \\ P_e &= 0.35 \text{ p.u.} \end{aligned} \quad (14)$$

Based on the chosen torsional modes and the initial operating condition, the real part of the resulting full impedance matrix, defined in (7), is depicted in Figure 7. Almost zero mechanical damping is assumed here for the subsynchronous torsional modes, although a small mechanical damping always exists in reality.

Consider further the standard control structure shown in Figure 5. Based on the resulting full impedance matrix \mathbf{Z}_{full} and the standard control structure, two simulation scenarios are performed in the following. In the first scenario, the control parameters are tuned such that the stability condition (9) is **not** satisfied for some of the chosen torsional modes. In the second scenario, the stability condition (9) is satisfied for all frequencies of interest. In this manner, the effect of the

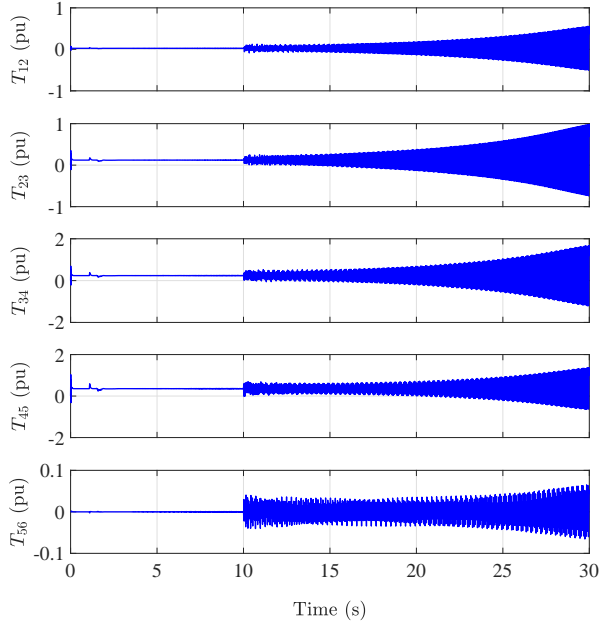


Figure 8. Resulting torsional torques for the first scenario

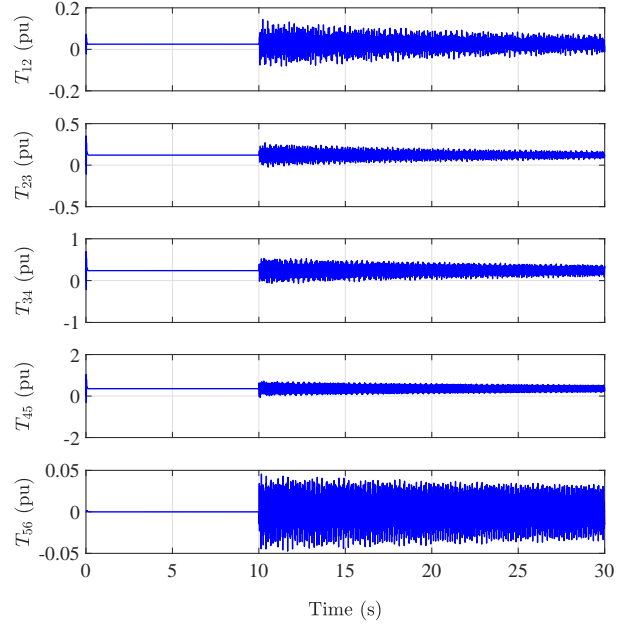


Figure 10. Resulting torsional torques without HVDC

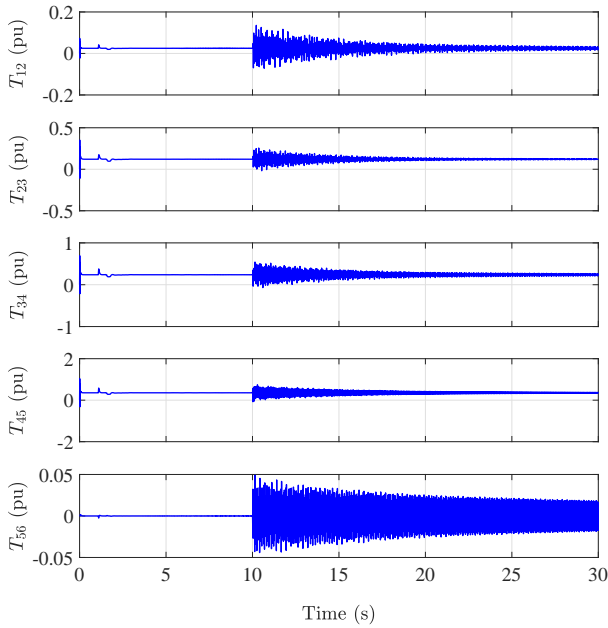


Figure 9. Resulting torsional torques for the second scenario

resulting harmonic impedance on the torsional modes can be measured from the stability preservation perspective.

The simulation results for the first scenario are depicted in Figure 8. The ac system is subject to a three-phase fault disturbance impulse at time instant $t = 10$ s. As expected, the ac system can not recover successfully. The simulation results for the second scenario, where the stability condition (9) is satisfied, for the same load flow are depicted in Figure 9. Obviously, the system stability is preserved while positively

contributing to the torsional damping. The ac system recovers successfully without any voltage/rotor stability issues. The positive damping effect of the HVDC has been evaluated by comparing it with the resulting torsional torques without HVDC. The results of the simulation scenario without HVDC are illustrated in Figure 10. A clearly damped behavior can be observed without HVDC, indicating the electrical positive damping contribution of the ac network itself. The magnitude of the resulting torsional torques with HVDC is however reduced much faster than without it.

To sum up, by satisfying the stability condition (9) not only stability of the system under study can be guaranteed but also its performance (measured by the torsional damping) can be improved as well.

V. CONCLUSIONS

A novel approach of modeling and analyzing MMC-based HVDC systems while considering the interactions with nearby turbine generators in the subsynchronous frequency range is proposed in this paper. The proposed approach is characterized by considering a so-called emulation-based design strategy with which the a stabilizing controller of the HVDC is first determined using classical control theory and then the stability of the system taking the mechanical dynamics of the turbine generator into account is studied. The effectiveness of the proposed theory is illustrated for a detailed representation of the MMC-based HVDC system in the PSCAD environment, showing its ability to predict system resonance caused by the lack of stability margin.

REFERENCES

- [1] P. Kundur, *Power System Stability and Control*. New York: McGraw-Hill, 1994.
- [2] P. M. Anderson, B. L. Agrawal, and J. E. V. Ness, *Subsynchronous resonance in power systems*. John Wiley & Sons, 1999.
- [3] K. R. Padiyar, *Analysis of subsynchronous resonance in power systems*. Springer Science & Business Media, 2012.
- [4] H. Ghasemi, G. Gharehpetian, S. A. Nabavi-Niaki, and J. Aghaei, "Overview of subsynchronous resonance analysis and control in wind turbines," *Renewable and Sustainable Energy Reviews*, vol. 27, pp. 234–243, 2013.
- [5] L. Harnefors, "Analysis of subsynchronous torsional interaction with power electronic converters," *IEEE Transactions on Power Systems*, vol. 22, no. 1, pp. 305–313, 2007.
- [6] —, "Proof and application of the positive-net-damping stability criterion," *IEEE Transactions on Power Systems*, vol. 26, no. 1, pp. 481–482, 2011.
- [7] N. Prabhu and K. R. Padiyar, "Investigation of subsynchronous resonance with VSC-based HVDC transmission systems," *IEEE Transactions on Power Delivery*, vol. 24, no. 1, pp. 433–440, 2009.
- [8] M. Mohaddes, A. M. Gole, and S. Elez, "Steady state frequency response of STATCOM," *IEEE Transactions on Power Delivery*, vol. 16, no. 1, pp. 18–23, 2001.
- [9] J. Sun, "Impedance-based stability criterion for grid-connected inverters," *IEEE Transactions on Power Electronics*, vol. 26, no. 11, pp. 3075–3078, 2011.
- [10] M. Céspedes and J. Sun, "Impedance shaping of three-phase grid-parallel voltage-source converters," in *Proceedings of the 27th IEEE Conference and Exposition on Applied Power Electronics*, 2012, pp. 754–760.
- [11] L. Harnefors, M. Bongiorno, and S. Lundberg, "Input-admittance calculation and shaping for controlled voltage-source converters," *IEEE Transactions on Industrial Electronics*, vol. 54, no. 6, pp. 3323–3334, 2007.
- [12] A. Radwan and Y. Mohamed, "Modeling, analysis, and stabilization of converter-fed ac microgrids with high penetration of converter-interfaced loads," *IEEE Transactions on Smart Grid*, vol. 3, no. 3, pp. 1213–1225, 2012.
- [13] Z. Miao, "Impedance-model-based SSR analysis for type 3 wind generator and series-compensated network," *IEEE Transactions on Energy Conversion*, vol. 27, no. 4, pp. 984–991, 2012.
- [14] L. Xu and L. Fan, "Impedance-based resonance analysis in a VSC-HVDC system," *IEEE Transactions on Power Delivery*, vol. 28, no. 4, pp. 2209–2216, 2013.
- [15] M. Tabbara, D. Nešić, and A. R. Teel, "Networked control systems: Emulation-based design," in *Networked control systems*. Springer, 2008, pp. 57–94.
- [16] IEEE SSR working group, "First benchmark model for computer simulation of subsynchronous resonance," *IEEE Transactions on Power Apparatus and Systems*, vol. 96, no. 5, pp. 1565–1572, 1977.
- [17] S. Debnath, J. Qin, B. Bahrani, M. Saedifard, and P. Barbosa, "Operation, control, and applications of the modular multilevel converter: A review," *IEEE Transactions on Power Electronics*, vol. 30, no. 1, pp. 37–53, 2015.
- [18] M. A. Perez, S. Bernet, J. Rodriguez, S. Kouro, and R. Lizana, "Circuit topologies, modeling, control schemes, and applications of modular multilevel converters," *IEEE Transactions on Power Electronics*, vol. 30, no. 1, pp. 4–17, 2015.
- [19] R. C. Dorf and R. H. Bishop, *Modern control systems*, 11th ed. New Jersey: Pearson, 2008.
- [20] L. Harnefors, L. Zhang, and M. Bongiorno, "Frequency-domain passivity-based current controller design," *IET Power Electronics*, vol. 1, no. 4, pp. 455–465, 2008.
- [21] L. Harnefors, A. G. Yepes, A. Vidal, and J. Doval-Gandoy, "Passivity-based controller design of grid-connected VSCs for prevention of electrical resonance instability," *IEEE Transactions on Industrial Electronics*, vol. 62, no. 2, pp. 702–710, 2015.
- [22] L. Harnefors, X. Wang, A. G. Yepes, and F. Blaabjerg, "Passivity-based stability assessment of grid-connected VSCs – An Overview," *IEEE Journal of Emerging and Selected Topics in Power Electronics*, vol. 4, no. 1, pp. 116–125, 2016.